Phase-transition promoted thermoelectric textiles based on twin surface modified CNT fibers

Long Yu[1,2], Xinyu Liu[1,2], Boxuan Zhang[1], Huijie Hu[2], Kunlin Chen[1,2], Haoxuan Li[2], David J.S. Birch[3], Yu Chen[3] , Hua Qiu[2] and Peng Gu[1,2*]

1. Department of Light Chemical Engineering, Jiangnan University, Wuxi, P. R. China, 214122
2. Key Laboratory of Eco-Textiles (Ministry of Education), School of Textile Science and Engineering, Jiangnan University, Wuxi, 214122 P. R. China
3. Photophysics Group, Department of Physics, Scottish Universities Physics Alliance, University of Strathclyde, 107 Rottenrow, Glasgow G4 0NG,

Email:

Peng Gu: peng.gu@jiangnan.edu.cn; tommy861007@hotmail.com

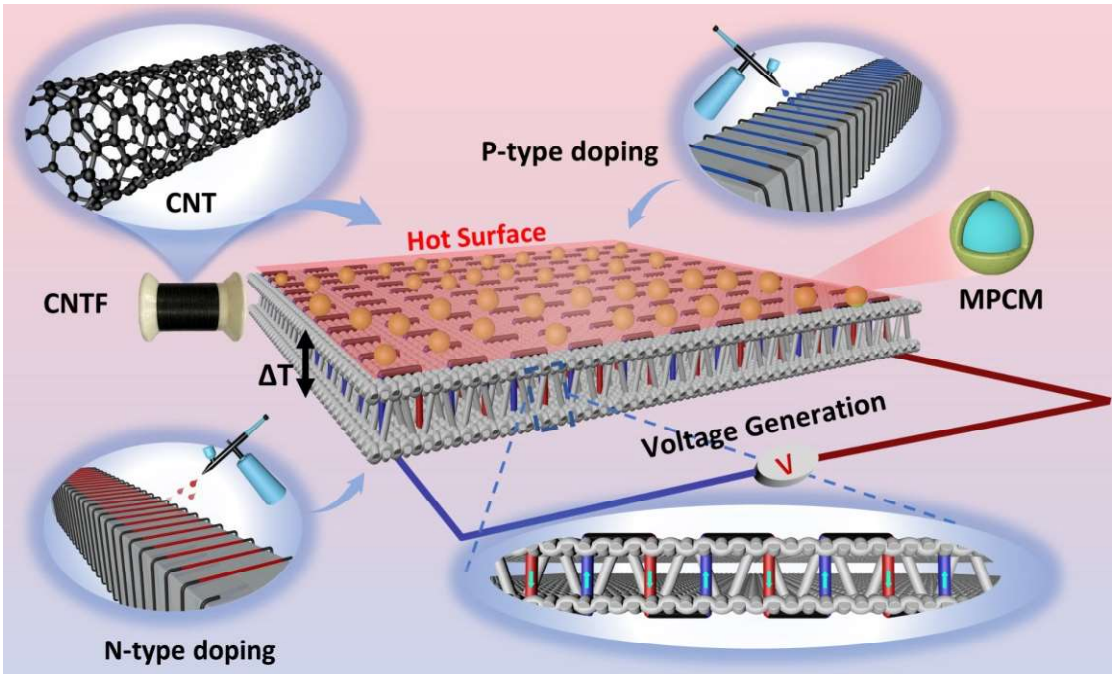

This is a peer-reviewed, accepted author manuscript of the following article: Yu, L., Liu, X., Zhang, B., Hu, H., Chen, K., Li, H., Birch, D. J. S., Chen, Y., Qin, H., & Gu, P. (2024). Phase-transition-promoted thermoelectric textiles based on twin surface-modified CNT fibers. ACS Applied Materials and Interfaces, 16(14), 18030–18039. https://doi.org/10.1021/acsami.4c00981

Abstract:

As the fast development of new science and technology, wearable devices are in great demand in modern human daily life. However, the energy problem is a long-lasting issue to achieve real smart, wearable and portable devices. Flexible thermoelectric generators (TEGs) based on thermoelectric conversion systems can convert body waste heat into electricity with excellent flexibility and wearability, which shows a new direction to solve this issue. Here in this work, polyethyleneimine (PEI) and gold nanoparticles (Au NPs) twin surface-modified carbon nanotube fibers (CNTF) were designed and prepared to fabricate thermalelectric textiles (TET) with high performance, good air stability and high-efficiency power generation. To better utilize the heat emitted by the human body, microencapsulated phase change materials (MPCM) were coated on the hot end of TET to achieve the phase-transition promoted TET. MPCM coated TET device could generate 25.7 % more energy than untreated control device, which indicates the great potential of the phase-transition promoted TET.

Key words: CNT, gold nanoparticles, thermoelectric textiles, twin-surface modification, microencapsulated phase change materials

1．Introduction

As a massive energy reservoir the human body releases massive and ubiquitous energy in daily life. Collecting and utilizing this sort of waste energy is vital important in the development of wearable electronic devices[1,2]. Importantly, the waste heat dissipated by the human body is continuous. Flexible and wearable TEG based on thermoelectric conversion systems can convert body waste heat into electricity with excellent flexibility and wearability which is a promising candidate to solve the energy problem on wearable devices[3-5]. In addition, TEG is also considered to have the potential to achieve fire warning due to the thermoelectric effect, and can be used in fire clothing and home life[6,7]. In the past few decades, flexible thermoelectric devices have developed rapidly[8]. Due to their excellent conductivity and controllable Seebeck coefficient (thermal power), carbon nanotubes (CNTs) materials are promising

alternatives to traditional inorganic thermoelectric materials[9,10]. Most flexible TEGs based on CNTs are manufactured by alternately stacking or printing P-type and N-type CNT films or inks, and depositing metal as electrodes between P-type and N-type elements[11,12]. However, connecting P-type and N-type legs through metal electrodes increases the contact resistance, which tends to reduce the output power of thermoelectric generators to some extent[13]. Therefore, flexible TEGs are usually assembled by arranging or stacking a series of thin films in-plane, which is an essential 2D structure and only able to collect heat energy in the in-plane direction[14,15]. However, the temperature gradient between the human body and the environment is mainly in the vertical direction, and this 2D structure of the P-N legs is difficult to meet the thermoelectric conversion in the vertical direction. Therefore, developing TEG with vertical structure will become more practical. For example, Chen et al. developed a three-dimensional spring-like thermoelectric device to meet the efficient conversion of temperature gradients on vertical structures[16,17].

As an alternative, CNTF have become an ideal choice for flexible wearable TEGs due to their excellent conductivity, flexibility, light weight, and scalability[18]. They can be easily combined with textiles to transform 2D structures into 3D structures, achieving high-efficiency thermoelectric conversion in the vertical direction between the human body and the environment. Typically, to improve the conversion efficiency of the TEG, the typical structure consists of P-type and N-type legs[19]. CNTF exhibits P-type semiconductor properties in an oxygen-rich environment, and it is necessary to improve both the P-type to N-type properties through doping[12]. In addition, the annealing process before and after doping has been proven to be an effective method to improve the thermoelectric performance of N-type CNTs[20,21]. Though TEG can convert heat into electricity, they exhibit low conversion efficiency, restricting the complete utilization of heat energy emitted by the human body. Phase change materials (PCMs), capable of absorbing and releasing energy based on their phase change temperature, are extensively utilized in heat storage and temperature regulation applications. Hu et al. integrated PCMs with TEGs of varying melting points to accomplish temperature regulation in diverse environments[22]. Leveraging the energy absorption and release

properties of PCMs, it may be feasible to attain superior energy efficiency in the TE sector. In thermoelectric performance, the power factor is related to both the Seebeck coefficient and electrical conductivity ($PF = S^2\sigma$, where S is the Seebeck coefficient and σ is electrical conductivity)[23]. Therefore, balancing the relationship between the two is crucial to improving device performance. Au NPs due to their low impedance, high electronegativity and enhanced chemical inertness have been used to improve the electrical and thermal conductivity of some materials[24,25]. In particular, when introducing Au NPs into CNTs components, the interface thermal and electrical transfer (ITT and IET) can be significantly improved[24]. Thus, it is hypothesized that when decorating CNTF with Au NPs, the Au NPs as a P-type dopant can enhance the electrical conductivity and Seebeck coefficient of CNTF, thereby improving the power factor.

Here in this work, PEI and Au NPs twin surface-modified CNTF were designed and prepared to fabricate TET with high performance, good air stability, heat storage, and high-efficiency power generation through multi-step processing. The influence of annealing before and after doping on the N-type thermoelectric performance was compared. The results showed that annealing treatment could improve the electrical conductivity of CNTF. Doping with PEI after annealing increased the power factor of the N-type legs up to 900 $\mu W\ m^{-1}\ K^2$, while annealing after PEI doping further increased the power factor to 1400 $\mu W\ m^{-1}\ K^2$. Meanwhile, the N-type legs maintained stable N-type properties even after exposure to air for 108 hours, indicating excellent air stability. For the P-type legs, introducing Au NPs with $HAuCl_4 \cdot 3H_2O$ significantly increased the electrical conductivity of the annealed P-segment, compensating for the decrease in P-type thermoelectric performance caused by annealing. In addition, to better utilize the heat emitted by the human body and improving the thermoelectric conversion efficiency, it is neccessary to simultaneously convert thermal energy into electrical energy while storing excess heat to achieve higher energy utilization. Microencapsulated phase change materials (MPCM) have great potential in waste heat utilization, temperature control and electronic cooling[26,27]. Therefore, melamine-formaldehyde resin microencapsulated octadecane and paraffin, were prepared and coated on surface of the

TET, achieving larger energy conversion and heat storage functions. The as-prepared TET integrated 72 PN segments and MPCM surface coatings could output a maximum power of ~270 nW at ΔT=6.6 K.

2 . Experimental Section

2.1 Materials

CNTF were synthesized in one step via floating catalyst chemical vapor deposition (FCCVD). PEI and $HAuCl_4 \cdot 3H_2O$ were provided by Shanghai Aladdin Reagent Co., Ltd. Paraffin, n-octadecane, melamine, formaldehyde (37 % aqueous solution), and ethanol were provided by China National Pharmaceutical Group. All chemicals were used as received without further treatment.

2.2 Preparation of P-N Structured CNTF.

The CNTF was spun continuously by the FCCVD method. Briefly, ethanol was used as the carbon source, ferrocene was used as the catalyst, and thiophene was used as the promoter to decompose the carbon source at high temperature under nitrogen and argon to form aerogel-like CNTs, which were then twisted and spun into CNTF.

The preparation method of CNTs thermoelectric fiber with P-N junction structure is shown in Fig. 1a, which mainly includes three steps: (1) PEI doping on a support unit consisting of a silicone strip with dimensions of 4×4×80 mm; (2) annealing at 200 ℃; (3) Au NPs modification. The detailed methods are as follows.

For N-type doping, the electric spray method was used to use different concentrations of PEI as the N-type dopant for CNTF. Specifically, PEI ethanol solutions with mass concentrations of 1 %, 5 %, 10 %, and 20 % were prepared and sprayed onto CNTF at a rate of 50 μL cm^{-1}. The samples were then dried for 5 minutes in air at 65 ℃. The spraying process was carried out carefully to avoid PEI penetration onto the P-type segment. The resulting PEI-doped CNTF was named as PEI/CNTF.

Subsequently, the N-type-doped CNTF was heated to 200 ℃ at a rate of 3 ℃/min in an argon atmosphere, maintained at 200 ℃ for 2 hours, and then cooled to room temperature. The CNTF treated with PEI after annealing was named as PEI/CNTF-A. In addition, a group of CNTF treated with annealing first and then with PEI was set as

a comparison. Note that only the order of PEI doping and annealing was changed, while the other steps remained the same. The CNTF processed by this process was named as A-PEI/CNTF.

For P-type doping, different mass concentrations of $HAuCl_4 \cdot H_2O$ solution (0.1 %, 0.5 %, 1 %, and 10 %, w/v) were sprayed onto P-annealed CNTF. Similarly, the samples were sprayed at a rate of 50 μL cm^{-1} and then dried for 5 minutes in air at 65 ℃. The samples were then cooled to -11℃ and circulated three times to completely reduce Au^{3+} to Au^0.

2.3 Preparation of MPCM

Preparation of emulsion: 3.4 g of octadecane and 0.6 g of paraffin were added to a 0.2 % (w/v) solution of sodium dodecyl benzene sulfonate. The mixture was heated until the solids were completely melted. The mixture was then homogenized with a homogenizer and ultrasonicated in a water bath for 10 minutes until the solution was uniformly mixed.

Preparation of prepolymer: 1 g of melamine and 2.15 g of formaldehyde were ultrasonicated for 10 minutes until completely dispersed, then diluted with 30ml of deionized water. The pH was adjusted to 8-9 using a 10 wt% solution of triethylamine and stirred at 60 ℃. After the solution became completely clear and transparent, stirring was continued for another 30 minutes.

Preparation of MPCM: The emulsion was poured into a three-neck flask, and the pH was adjusted to 3-4 with a 10 wt% HCl solution. Prepolymer was slowly added and stirred for 10 minutes at room temperature. The reaction was carried out at 70 ℃ for 3 hours. The resulting product was washed three times with deionized water and ethanol, and dried at 40 ℃ in air.

2.4 Preparation of flexible CNTF-based TET.

The CNTF marked with silver paste was wrapped around a silicone strip to distinguish the P-segment and N-segment, and then carefully sewn onto a fabric to form a π-junction structure. The inner side of the fabric was soaked in a 50% MPCM solution for 10 minutes, then dried at 70 ℃ to obtain MPCM/TET, with one side of the MPCM in contact with the hot end.

2.5 Characterization and Performance measurements.

Field-emission scanning electron microscopy (FESEM, SU8100, Hitachi High-Technologies Corporation, Japan) was utilized to characterize the morphology of the pristine CNTF, doped CNTF, and phase-change microcapsules. A confocal Raman microscope (inVia Reflex, Renishaw, UK) was employed using a 532 nm laser wavelength to assess the degree of defects in the CNTF. An X-ray photoelectron spectrometer (XPS, Thermo SCIENTIFIC ESCALAB 250X) was employed to analyze the chemical state and the peak fitting of XPS spectra is carried out using Avantage software. The phase transition characteristics of the microcapsules were analyzed using a differential scanning calorimeter (DSC, Mettler DSC3+, Mettler Toledo, Switzerland) with a heating/cooling rate of 3 °C min^{-1} under nitrogen atmosphere. All samples were tested within a temperature range of 0°C to 60°C. Thermal gravimetric analysis (TG, Mettler TGA2, Mettler Toledo, Switzerland) was performed on the microcapsules using a fully automated TGA instrument in the temperature range of 0 °C to 800 °C.

The electrical conductivity σ (S cm^{-1}) was calculated using the formula σ=L/RS, where L represents the length (cm), and S represents the cross-sectional area (cm^2) obtained by measuring the diameter of CNTF at five locations in FESEM images and averaging them. The resistance R was measured using a Keithley 6510 digital multimeter (Keithley Instruments, Inc., USA) at room temperature. The average of five measurements was used for data analysis. The Seebeck coefficient (S) was calculated using a self-made apparatus (Figure S1) according to the equation $S=-\Delta V/\Delta T$, where the potential difference ΔV was monitored using a Keithley 6510 digital multimeter (Keithley Instruments, Inc., USA), and the temperature difference ΔT was monitored using an infrared thermal imaging camera (DL700, Dali Technology, China) at ten different thermal gradients to reduce errors. The linear correlation (R^2) between ΔV and ΔT was expected to be greater than 0.999. The open-circuit voltage of TET was monitored using a Keithley 6510 digital multimeter at room temperature, and the temperature difference between the upper and lower ends of TET was recorded using a K-type thermocouple thermometer (TA612C, Suzhou Teans Electronics Industry Co., Ltd.). The U-I curve of TET was measured using an electrochemical workstation (CS150H, WUHAN CORRTEST INSTRUMENTS CORP., LTD.), and the power was

calculated using the formula P=UI. The cyclic folding test of TET was performed using an electric force gauge (ESM303, MARK-10 Co., Ltd., USA).

3 Results and Discussion

3.1 Preparation of PEI and Au NPs twin surface-modified CNTFs

The original CNTF had P-type semiconductor characteristics due to their adsorption of oxygen in the air[28,29]. To enhance the Seebeck effect of the TET, it was necessary to chemically modify the CNTF from P-type to N-type. Common doping methods for CNTs include substitutional doping[19], and adsorption-based doping. In substitutional doping, dopant atoms replace carbon atoms, while in adsorption-based doping, dopant molecules adsorb onto CNTs surfaces to induce surface charge transfer and achieve N or P-type doping. Adsorption-based charge transfer doping is an effective method for doping CNTs without compromising their structure[18].

Figure1a illustrates the process of alternating P/N doping in a single CNTF. For N-type CNTF, the spray amount was controlled at 200 μL. Subsequent annealing was conducted to deoxygenate the CNTF, but the temperature was carefully controlled to prevent thermal degradation of the PEI dopant. Therefore, annealing was performed to deoxygenate the CNTF, but the temperature was kept below the boiling point of PEI (250℃). By adjusting the annealing temperature and time, the conductivity and Seebeck coefficient of N-type CNTF under different treatment conditions were obtained. Finally, the temperature and time were determined to be 200℃ and 2h (Figure S2). The surface of the original CNTF exhibited a well-defined network structure of intertwined CNT bundles that was revealed through cross-sectional imaging techniques as shown in Figure 1b. However, after surface treatment with PEI and chloroauric acid, the distinctive network structure became less apparent. In particular, the PEI treatment resulted in a marked increase in the degree of CNTs bundling and cross-linking, leading to the formation of a more dispersed and irregular morphology within the CNTF matrix, as evidenced by cross-sectional SEM imaging as shown in Figure 1c and d. The diameter of the PEI-treated CNTF was 118.42 μm, which was slightly thicker than the original diameter of 113.14 μm (Figure S3). As shown in Figure 1e-g, EDS analysis

revealed the presence of characteristic elements within the CNTF matrix, including the C atoms in the CNTs themselves, N atoms in the PEI N-type dopant, and Au atoms in the $HAuCl_4 \cdot 3H_2O$ P-type dopant. The uniform distribution of these elements throughout the matrix provided strong evidence for the successful doping and integration of the dopants into the CNTF network.

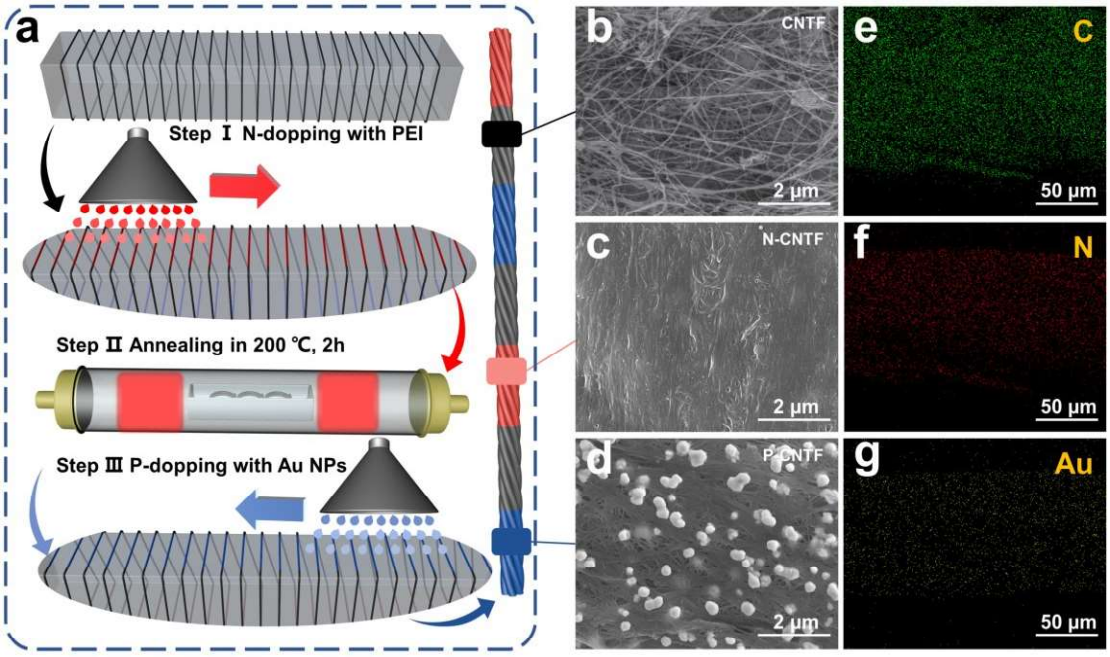

Figure 1. (a) Schematic diagram of P- and N-doping of the CNTF legs. (b-d) SEM images of CNTF surface before and after doping. (e-g) The EDS results distinguish the different segments by mapping their characteristic elements (carbon C from pure CNTF, nitrogen N for PEI modified CNTF, and Au for Au NPs modified CNTF).

As shown in Figure 2a-c and Figure S4a, an XPS was employed to prove the successful surface modification of PEI. Obvious peaks of the elements C, N, O can be detected after PEI modification. A peak in the N1s orbital can be seen, which indicates the successful doping of PEI (Figure 2a). The C1s peaks reveal that the main peak is fitted with three peaks at 284.7 eV, 286.4 eV and 288.7 eV, respectively (Figure 2b). The peak at 284.7 eV is attributed to the sp2 hybridized carbon atoms (C–C)[29]. The peaks at 286.4 eV and 288.7 eV are C=C bonds and C–O bonds[20,30]. After PEI surface doping, the C-O bounds are mostly replaced by C-N bounds, which are shown in Figure 2c and indicates the succesful PEI surface modification. These data provided robust and reliable evidence for the successful doping and integration of the dopants into the CNTF

matrix for N-type legs. A contrast among the Raman spectra of pristine CNTF, CNTF-A, PEI/CNTF-A and A-PEI/CNTF are shown in Figure S4b. The spectra display two typical bands at around 1324 cm^{-1} (D-band) and around 1573 cm^{-1} (G-band), which corresponds to the structural defect and crystalline nature of CNTs, respectively[8,20].As can be seen, the intensity ratio (I_D/I_G) from 0.36 turns to 0.16 after subsequent annealing process, indicating that the annealing process can reduce the defect in CNTs. This result accounts well for the enhancement in the electrical conductivity after annealing process. While the value of I_D/I_G slightly increases from 0.16 to 0.19 after PEI doping, which suggests a covalent as well as noncovalent interaction between PEI molecule and CNTs[8].

For P-type legs, the XRD analysis was also carried out to confirm the structural integrity of the CNTF matrix, as evidenced by the distinct C (002) and Au (111), (200), (220), (311) and (222) diffraction peaks as shown in Figure S4c [24]. These peaks, which were well-resolved, sharp, and characteristic of highly crystalline structures, strongly indicated the presence and proper incorporation of the Au NPs into the CNTF matrix. The combination of EDS and XRD techniques thus provided robust and reliable evidence for the successful doping and integration of the dopants into the CNTF matrix for N-type legs and P-type legs.

The legs of the TET with a P-N structure can generate a small open-circuit voltage under a temperature gradient, as the temperature difference between two different conductors or semiconductors results in a potential difference, known as the Seebeck effect (shown in Figure S5). For n-type doping, the electric spray method was used for different concentrations of PEI as the N-type dopant for CNTF. Specifically, PEI ethanol solutions with mass concentrations of 1 %, 5 %, 10 %, and 20 % were prepared and sprayed onto CNTF at a rate of 5 μL s^{-1}. The original CNTF exhibits a positive Seebeck coefficient, but after annealing, the N-type performance is enhanced due to oxygen desorption, resulting in a decrease in the Seebeck coefficient[20]. The effects of annealing and PEI treatment in different orders on the TE performance of CNTF were compared in Figures 2e-f. As shown in Figure 2e-f, PEI doping followed by annealing

has higher Seebeck coefficient and electrical conductivity. A pronounced enhancement in Seebeck coefficient from −38 μV K^{-1} to −80 μV K^{-1} in the case of 10% PEI concentration is achieved, and the electrical conductivity increase from 1200 S cm^{-2} to 2100 S cm^{-2}. The subsequent annealing process can thereby be served as a second N-doping process, the increase in the Seebeck coefficient is due to the annealing process could also deplete the hole near the valence band of CNTs and upshift the Fermi energy level toward the conduction band by desorbing the oxygen[31].These effective treatments ncrease the power factor of PEI/CNTF-A to ~ 1400 μW m^{-1} K^{-2} (Figuer 2f). Interestingly, according to Figure S6a, the Seebeck coefficient after PEI doping followed by annealing treatment remains almost constant even being exposed to air for over 100h, which indicates the TET has superior air stability.

For P-type doping, different mass concentrations of $HAuCl_4 \cdot 3H_2O$ solution (0.1 %, 0.5 %, 1 %, and 10 %, w/v) were sprayed onto P-type CNTF. As shown in Figure 2g, $HAuCl_4 \cdot 3H_2O$ doping can compensate the drop in Seebeck coefficient resulted from the annealing process, and the maximum Seebeck coefficient value of ~58 μV K^{-1} is achieved at 1% concentration. The electrical conductivity of P-type CNTF increases with the increase of $HAuCl_4 \cdot 3H_2O$ concentration (Figure 2h), which is because that Au NPs started to act as an effective, strong and electrically conductive bridge to interconnect CNT bundles for the facilitated load and electron transfer[25]. Although the electrical conductivity has been increasing, the Seebeck coefficient reaches its maximum value at 1% concentration, resulting in a maximum power factor of ~ 2100 μW m^{-1} K^{-2} at 1% concentration (Figure 2i). In comparison with the power factor of N-type and P-type materials prepared by different methods reported in other literature, including wet spinning, CVD spinning and composite materials, the CNTF power factor prepared in this study is still quite high. And the original CNTF exhibits high conductivity and Seebeck coefficient, and reasonable doping is necessary to achieve high PF performance in both organic and inorganic(Figuer S4d).

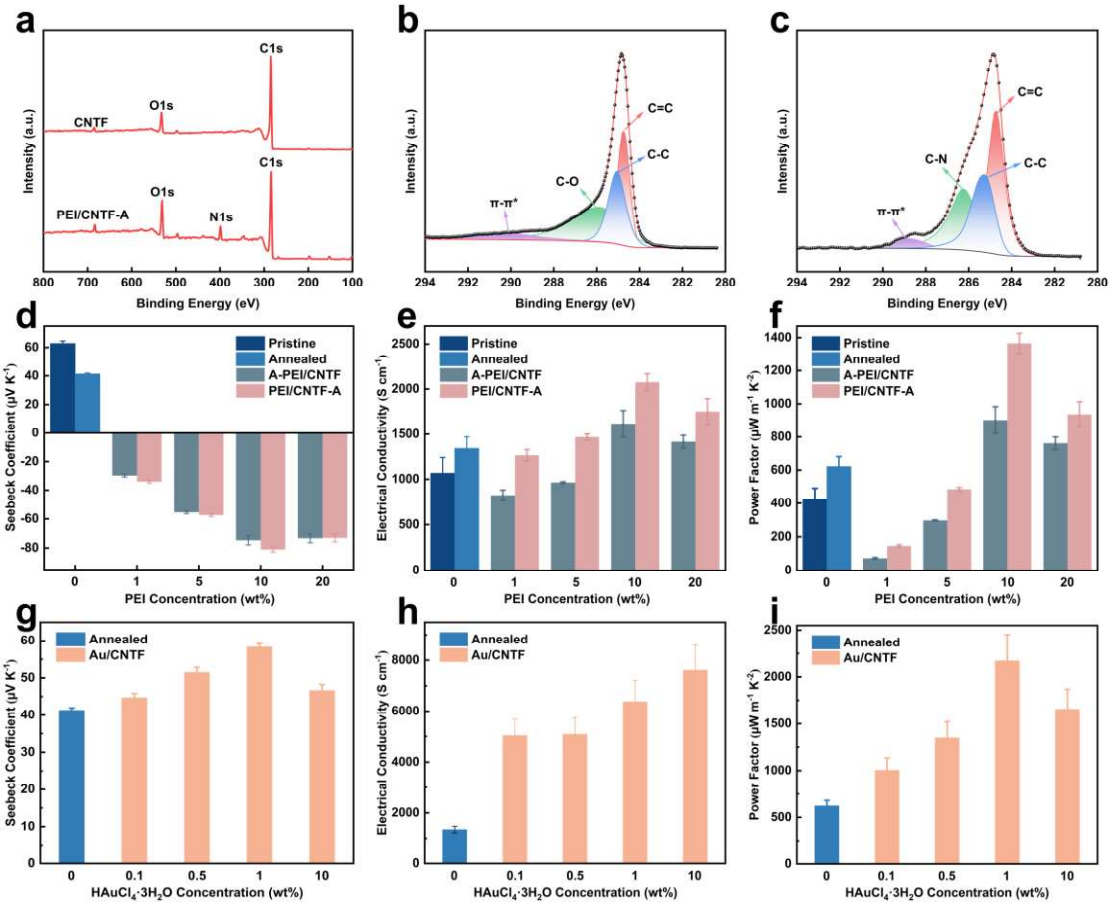

Figure 2. (a) The full XPS spectra of pristine CNTF and PEI/CNTF-A. (b,c) The high resolution of C1s XPS spectra ofpristine CNTF and PEI/CNTF-A. (d-f) Seebeck coefficient, electrical conductivity and power factor versus concentration of N-type dopant and subsequent annealing process, respectively. (g-i) Seebeck coefficient, electrical conductivity and power factor versus concentration of P-type dopant respectively.

3.2 CNTF based TET

After the successful preparation the P-N doped CNTF were carefully removed from the flexible silicone substrate and sewn onto a spacer fabric measuring 70 mm × 50 mm × 4 mm (length × width × height) to fabricate the TET (Figure 3a and b). The spacer fabric was designed with a height matching that of the P-N doped CNTF, enabling them to be well-hidden within the fabric while exposing the undoped regions to the heat source and forming a π-type structure based on the fiber orientation. The spacer fabric played a critical role in improving the TET performance by ensuring uniform heat

distribution and reducing the heat transfer of the device[30]. In the meantime, the device shows excellent flexibility of bending, twisting and pressing as shown in Figure 3c.

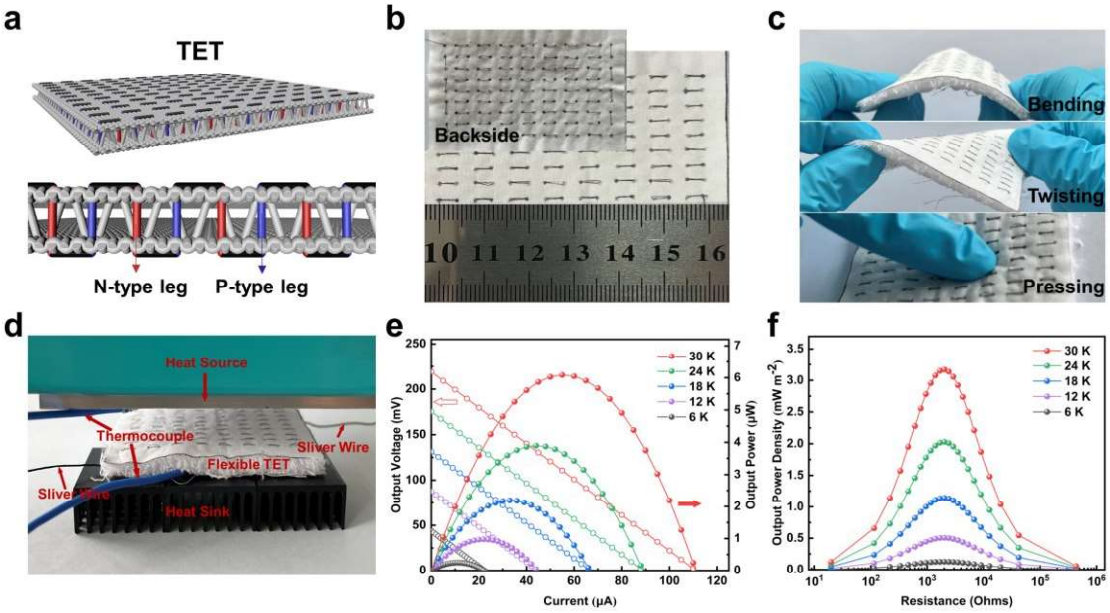

Figure 3. (a) Schematic diagram of the plan and section of the spacing fabric-based TET. (b) Front and backside photograph of a spacer fabric-based TET with 72 PN pairs. (c) Photograph depicting easy bending, twisting and pressing of the TET. (d) Photograph showing an apparatus of power measurement system. (e) Output voltage and output power of the TET with 72 PN pairs as a function of the temperature gradient. (f) Output power density of the TET with respect to the external resistance R at various temperature differences.

To evaluate the practical performance of the TET, the output voltage and the output power were measured at ΔT of 6−30 K using the apparatus shown in Figure 4d, including TET, heat sources, silver conductive wire, thermalcouple and heat sink. Notably, the TET with 72 PN pairs exhibited an maximum output voltage of 43.8 mV and 219.1 mV while the maximum output power was 0.24 μW and 6.1 μW at ΔT=5 K and 30 K, respectively (Figure 3e). Meanwhile, Figure 3f shows the output power density of the TET devices under various external load R at different temperature differences.-The maximum output power density P_{max} of the TET was 3.17 mW m^{-2} at ΔT = 30 K as R = 2.01 kΩ.

When directly pressing with the hand under ambient conditions (ΔT=6.6 K), the TET with 72 PN pairs generates the output voltage of 42.65 mV (Figure 4a). The CNTF-

based TEG effectively harvests human body heat, even from curved surfaces such as the forearm.As shown in Figure 5b, the output powers were 261.5 nW and 124.7 nW on the hand and forearm, respectively. Figure 4c shows the time-resolved voltage of the TET devices attached to a human's hand and forearm and the insert is a thermal IR camera image of a hand. After 10 s the output voltage is more likely to be stable, the generated voltages gradually decrease when thermal equilibrium is reached after ≈100 s, and the overall dropping rate after 100 s for TET devices on the hand and forearm were 21.1 % and 26.6 %, respectively, which indicates the great potential on wearable energy generation.

To verify the heat phemonema of the TET device under the touch of hand a finite element analysis (FEA) simulation was performed to predict the heat distribution at different moments. Figure 4d shows the FEA results of the temperature distribution at different time points. The environment temperature was 298 K and the ΔT = 6 K, in order to get a more accurate result and Figure 4e further confirmed the simulation result. As soon as the hand touched the TEG, the output voltage was immediately generated, and it continuously increased with the contact time (Figure 4e). As the touch of TET device by hand, open voltage accured immediately and kept increasing to 39 mV for 5 s of consistent touching. After disconnecting the hand after 5 s the voltage dropped dramtically to 0 after 40 s. To further explore its temperature sensing capability, the TET was brought into contact with heat sources at different temperatures, and the time-resolved open-circuit voltage was measured (Figure 4f). As the TET was brought into contact with targets of a higher temperature, the resulting output voltage increased correspondingly. It should be noted that a negative output voltage was measured when the target temperature was lower than that of the ambient temperature. These results demonstrate the possibility of utilizing our TET as wearable high-resolution temperature sensors with fast responses.It could be found from Figure 4h that the device displays a quick response to the hand temperature. In addition, a stable amplitude of ~35 mV in voltage response can be sustainably obtained during multiple fingering cycles. The CNTF-based TET shows excellent flexibility and durability with no

significant changes in the device resistance and output voltage under mechanical deformation, even after 3000 bending cycles (Figure 4h). Furthermore, when the TET undergoes repeated cycles of folding and twisting, its resistance and voltage changes are insignificant. After 100 cycles of testing, the TET exhibited a consistently stable resistance and voltage output(Figure S6b and c).

Figure 4i and Table S1 illustrate the normalized output performance for comparison to the other TEGs. By exploiting the enhanced TE properties of the Au NPs and PEI-doped CNTF and high fill factor of the serially connected PN-legs enabled, our highly integrated TET exhibits the highest normalized output voltage per unit area of 0.37 mV K^{-1} cm^{-2} among the many TEGs[16,18,32-40]. Moreover, our pro-posed TET also marks one ofthe highest normalized power density (3.5 × 10−4 μW K^{-2} cm^{-2}) when compared to TEGs based on organic and inorganic TE materials or CNTs, which demonstrate the thermal regulation effect of TET prepared based on spacer fabrics.

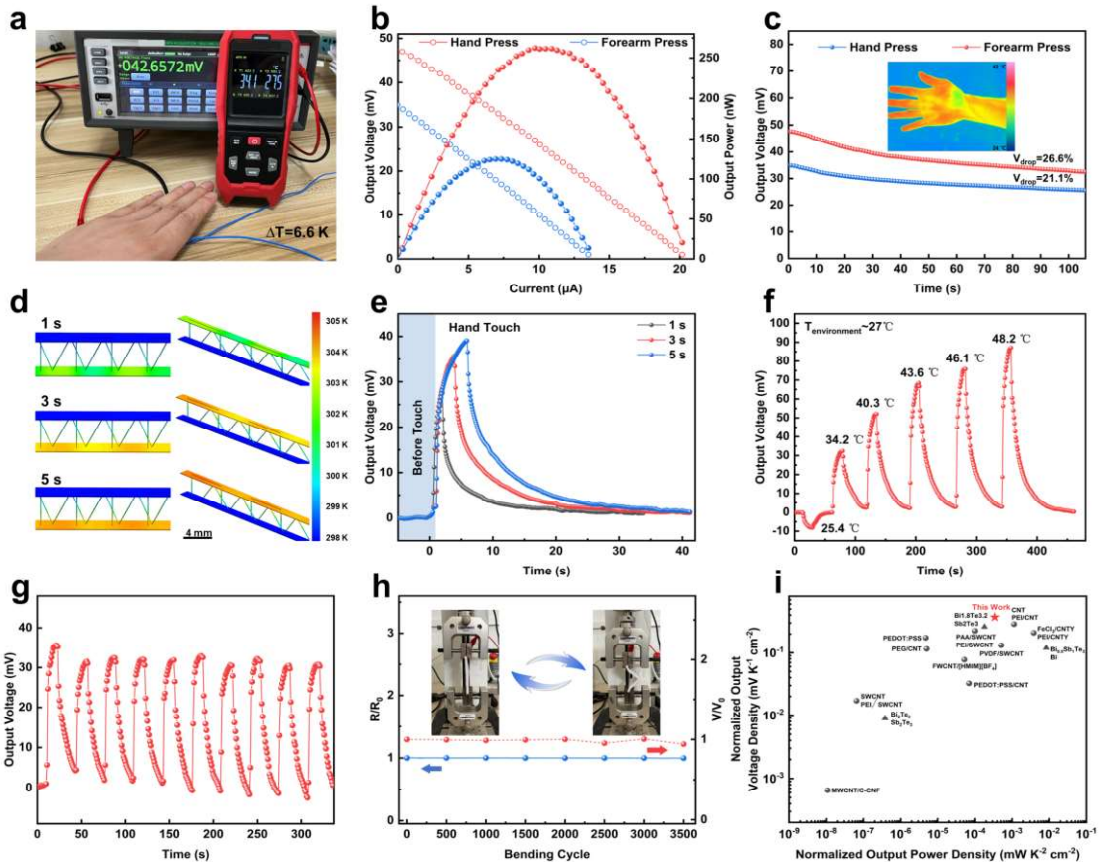

Figure 4. (a) Output voltage of TET obtained from the temperature difference between body heat and the surrounding atmosphere. (b) Output voltage and output power of the

TEG at the temperature difference between the hand or forearm. (c) Output voltage of the TEG over time. (d) Schematic of the finite element analysis of the temperature gradient formed at the TE legs after 1 s,3 s and 5 s of contact with a curved surface. (e) Time-resolved output voltage curve along hand contact time. (f) Measured the time-resolved voltage with a change in the temperature of the contact target. (g) The real-time response of voltage during multiple cycles. (h) Resistance and output voltage changes of the TEG versus number of bending cycles at a bending radius of 4 cm. (i) Comparison of output power densities of the TEGs in this work and recent reports.

3.3 Phase-transition promoted TET

Heat balance is a big issue for TE devices, which hinders the further development and application of TE devices in reality[27]. As the time goes by the device could achieve a balanced temperature leading dramatically to the voltage reduction to zero. To better utilize the heat emitted by the human body and improving the thermoelectric conversion efficiency, it is neccessary to simultaneously convert thermal energy into electrical energy while storing excess heat to achieve higher energy utilization[37]. MPCM have great potential in waste heat utilization, temperature control and electronic cooling[26]. Therefore, melamine-formaldehyde resin microencapsulated octadecane and paraffin, were prepared and coated on surface of the TET, achieving larger energy conversion and heat storage functions.

As shown in Figure 5a, the emulsion was poured into a three-neck flask, and the pH was adjusted to 3-4 with a 10 wt% HCl solution. Prepolymer was slowly added and stirred for 10 minutes at room temperature. The reaction was carried out at 70 °C for 3 hours to form the microencapsulated phase change materials (Figure S7a and b). Figure 5b shows the SEM image of a single MPCM. The corresponding elemental mappings are shown in Figure 5c, from which the uniform element distribution of N, O and C further confirmed the successful synthesis of MPCM. The phase change performance and heat stability of the microencapsulated octadecane were investigated by dynamic DSC and TG scans. The resulting data are shown in Figure 5d and Figure S7. It is found that MPCM exhibited a strong heat absorption over a broad range from 27 - 39 °C and

a strong heat release by an even boarder peak ranging from 0 - 27 °C. The MPCM melts at 30.6 ℃ in the heating process with a melting enthalpy of 106.38 J/g, and crystallizes at 20.2 ℃ and 14.4 ℃ in the cooling process with a crystallizing enthalpy of 153.03 J/g in the temperature range of 0 to 60 ℃. Meanwhile, the TG curves prove that the MPCMs were stable under 250 °C, which would almost never occur for wearable devices. These data above further indicate that the successfully synthesis of MPCMs and the MPCMs are extremely stable under mild working conditions. As described in section 2.4, a layer of MPCM was coated on the inner side of the TET device, which means that the microcapsules used are under a dirction contact to the human skin, the hot source. And the SEM image of Figure S8a proves the successful coating of MPCM on fabric fibers.

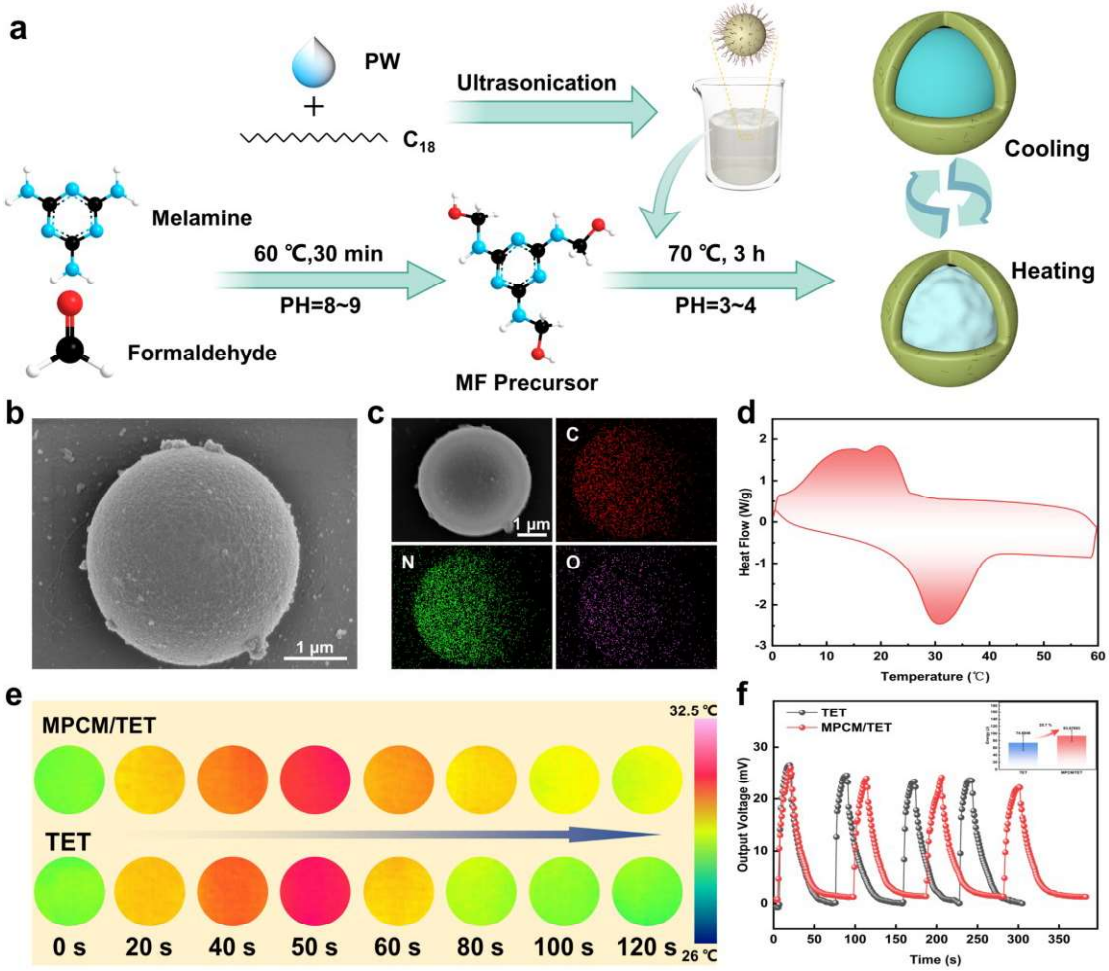

Figure 5. (a) Schematic diagram of MPCM preparation process. (b,c) SEM and mapping images of MPCM. (d) The DSC scan of MPCM in 0~60℃. (e) Thermal

infrared images of temperature rise and fall for TET and MPCM/TET. (f) The real-time response of output voltage of TET and MPCM/TET during multiple cycles. The illustration shows the energy utilization of TET and MPCM/TET in one cycle.

Figure S8b and c exhibits the temperature variation curve of MPCM treated and TET device and the output voltage and power of the MPCM/TEG wearing on the hand. The MPCM has a phase transition temperature of around 30°C, closely matching the hand's temperature. When the hand touches it, the material undergoes a phase change, absorbing some of the heat energy. Then, a portion of this heat energy is converted into electrical energy through the TET, directly. In the meantime, the phase change material stores some of the energy as well. When the palm leaves the TET, the heat source diminishes, causing the phase change material to undergo another transition, releasing the heat energy it absorbed earlier. This energy is then converted into a minor amount of electrical energy through the TET, thereby improving its performance. As shown in Figure 5f, under the hand touch condition, the MPCM coated TET device showed a lower surface temperature before the peak temperature as the phase transition materials absorbed the heat energy and was stored. After the peak point, the temperature started to drop and the MPCM coated TET device showed a higher temperature than the uncoated control sample, as the stored energy in phase transition materials is slowly released. These data are consistent with Figure 5e, which indicates the same temperature change process. Figure S8c showed that the as-prepared TET device integrated 72 PN segments and MPCM surface coatings could generate an output voltage and power of 39 mV verus 155 nW at ΔT=5 K. The inserted bar chart in Figure 5f also showed that the MPCM coated TET device could generate 25.7 % more than control untreated devices for the total energy generated for one circle, which indicates the great potential of the phase-transition promoted TET.

4. Conclusion

In conclusion, PEI and AuNPs twin surface-modified N-type and P-type CNTF were designed and prepared to fabricate TET with high performance, good air stability, heat storage, and high-efficiency power generation through multi-step processing. The

influence of annealing before and after doping on the N-type thermoelectric performance was compared. The results showed that annealing treatment could improve the TE performance of CNTF. Doping with PEI after annealing increased the power factor of the N-type legs up to 900 μW m^{-1} K^2, while annealing after PEI doping further increased the power factor to 1400 μW m^{-1} K^2. Meanwhile, the N-type legs maintained stable N-type properties even after exposure to air for 108 hours, indicating excellent air stability. For the P-type legs, introducing Au NPs with $HAuCl_4 \cdot 3H_2O$ significantly increased the electrical conductivity of the annealed P-segment, compensating for the decrease in P-type thermoelectric performance caused by annealing. In addition, to better utilize the heat emitted by the human body and improving the thermoelectric conversion efficiency, it is neccessary to simultaneously convert thermal energy into electrical energy while storing excess heat to achieve higher energy utilization. MPCM show great potential in waste heat utilization, temperature control and electronic cooling. Therefore, melamine-formaldehyde resin microencapsulated octadecane and paraffin were prepared and coated on the surface of the TET, achieving larger energy conversion and heat storage functions. The as-prepared TET integrated 72 PN segments and MPCM surface coatings could output a maximum power of ~270 nW at ΔT=6.6 K.

Supporting Information

Illustrations of TE performance measurements; Electrical conductivities, thermopowers, and power factors of the N-type CNTY (doped with 10wt% PEI) with annealing treatment at different temperatures and times; SEM images of CNTF; the high resolution of N1s XPS spectra of PEI/CNTF; Raman spectra of CNTF with different treatments; the XRD image of Au-doped CNTF; comparison of the power factors achieved in this work and recent reports on TE materials; schematic diagram of the Seebeck effect principle using thermoelectric power generation; air stability of N-type CNTF under different treatment methods; Resistance and output voltage changes of the TEG versus number of folding and twisting cycles; PW and C18 Pickering emulsions**;** SEM images of MPCM; TG curves of MPCM; SEM images of treated TET coatings based on MPCM; temperature variation curve of treated TET based on MPCM; output voltage and output power of the MPCM/TEG at the hand pressing; comparison of this

work with recent reports on the output power density of TEGs.

Author Contributions

P. GU and L. Yu conceived and designed the experiments. P. GU and L. Yu performed the experimental work and wrote the manuscript draft. X. Liu, B. Zhang and H. Hu helped with data collection and analysis and participated in the creation of figures. All authors discussed the results and contributed to manuscript writing and editing.

Notes

The authors declare no competing financial interest.

Acknowledgement

This work was financially supported by the National Natural Science Foundation of China (no. 52203226), Key Unveiling Project of Jiangxi Province (20213AAE02017), Knowledge Transfer Project of Jiangsu Province (no. 202202641) and the Fundamental Research Fund for Central Universities (JUSRP11918).

Reference

(1) Xiao, Y.; Zhao, L. D. Seeking New, Highly Effective Thermoelectrics. *Science* **2020,** 367 (6483), 1196–1197.

(2) Disalvo, F. J. Thermoelectric Cooling and Power Generation. *Science* **1999**, 285 (5428), 703–706.

(3) Yang, Q.; Yang, S.; Qiu, P.; Peng, L.; Wei, T. R.; Zhang, Z.; Shi, X.; Chen, L. Flexible Thermoelectrics Based on Ductile Semiconductors. *Science* **2022**, 377 (6608), 854–858.

(4) Jin, Q.; Jiang, S.; Zhao, Y.; Wang, D.; Qiu, J.; Tang, D. M.; Tan, J.; Sun, D. M.; Hou, P. X.; Chen, X. Q.; Tai, K.; Gao, N.; Liu, C.; Cheng, H. M.; Jiang, X. Flexible Layer-Structured Bi_2Te_3 Thermoelectric on a Carbon Nanotube Scaffold. *Nat. Mater*. **2019**, 18 (1), 62–68.

(5) Chen, W. Y.; Shi, X. L.; Zou, J.; Chen, Z. G. Wearable Fiber-Based Thermoelectrics from Materials to Applications. *Nano Energy* **2021,** 8, No. 105684.

(6) Li, G.; Hu, Y.; Chen, J.; Liang, L.; Liu, Z.; Fu, J.; Du, C.; Chen, G. Thermoelectric and Photoelectric Dual Modulated Sensors for Human Internet of Things Application in Accurate Fire Recognition and Warning. *Adv. Funct. Mater.* **2023,** 33 (41), No. 2303861.

(7) Jing, Y.; Luo, J.; Han, X.; Yang, J.; Liu, Q.; Zheng, Y.; Chen, X.; Huang, F.; Chen, J.; Zhuang, Q.; Shen, Y.; Chen, H.; Zhao, H.; Snyder, G. J.; Li, G.; Zhang, T.; Zhang, K. Scalable Manufacturing of a

Durable, Tailorable, and Recyclable Multifunctional Woven Thermoelectric Textile System. *Energy Environ. Sci.* **2023,** 16 (10), 4334–4344.

(8) Sun, T.; Zhou, B.; Zheng, Q.; Wang, L.; Jiang, W.; Snyder, G. J. Stretchable Fabric Generates Electric Power from Woven Thermoelectric Fibers. *Nat. Commun.* **2020,** 11 (1), 572.

(9) Yu, C.; Murali, A.; Choi, K.; Ryu, Y. Air-Stable Fabric Thermoelectric Modules Made of N- and P-Type Carbon Nanotubes. *Energy Environ. Sci.* **2012,** 5 (11), 9481–9486.

(10) Komatsu, N.; Ichinose, Y.; Dewey, O. S.; Taylor, L. W.; Trafford, M. A.; Yomogida, Y.; Wehmeyer, G.; Pasquali, M.; Yanagi, K.; Kono, J. Macroscopic Weavable Fibers of Carbon Nanotubes with Giant Thermoelectric Power Factor. *Nat. Commun.* **2021,** 12, 4931.

(11) Kumanek, B.; Stando, G.; Stando, P.; Matuszek, K.; Milowska, K. Z.; Krzywiecki, M.; Gryglas-Borysiewicz, M.; Ogorzałek, Z.; Payne, M. C.; MacFarlane, D.; Janas, D. Enhancing Thermoelectric Properties of Single-Walled Carbon Nanotubes Using Halide Compounds at Room Temperature and Above. *Sci. Rep.* **2021,** 11, 8649–8667.

(12) Lee, T.; Park, K. T.; Ku, B. C.; Kim, H. Carbon Nanotube Fibers with Enhanced Longitudinal Carrier Mobility for High-Performance All-Carbon Thermoelectric Generators. *Nanoscale* **2019,** 11 (36), 16919–16927.

(13) Ding, T.; Chan, K. H.; Zhou, Y.; Wang, X. Q.; Cheng, Y.; Li, T.; Ho, G. W. Scalable Thermoelectric Fibers for Multifunctional Textile-Electronics. *Nat. Commun.* **2020,** 11, 6006.

(14) Macleod, B. A.; Stanton, N. J.; Gould, I. E.; Wesenberg, D.; Ihly, R.; Owczarczyk, Z. R.; Hurst, K. E.; Fewox, C. S.; Folmar, C. N.; Holman Hughes, K.; Zink, B. L.; Blackburn, J. L.; Ferguson, A. J. Large N- and p-Type Thermoelectric Power Factors from Doped Semiconducting Single-Walled Carbon Nanotube Thin Films. *Energy Environ. Sci.* **2017,** 10 (10), 2168–2179.

(15) Mulla, R.; Jones, D. R.; Dunnill, C. W. Thermoelectric Paper : Graphite Pencil Traces on Paper to Fabricate a Thermoelectric Generator. *Adv. Mater. Technol.* **2020,** 1, 2–9.

(16) Liang, L.; Wang, M.; Wang, X.; Peng, P.; Liu, Z.; Chen, G.; Sun, G. Initiating a Stretchable, Compressible, and Wearable Thermoelectric Generator by a Spiral Architecture with Ternary Nanocomposites for Efficient Heat Harvesting. *Adv. Funct. Mater.* **2022,** 32 (15), No. 2111435.

(17) Lv, H.; Liang, L.; Zhang, Y.; Deng, L.; Chen, Z.; Liu, Z.; Wang, H.; Chen, G. A Flexible Spring-Shaped Architecture with Optimized Thermal Design for Wearable Thermoelectric Energy Harvesting. *Nano Energy* **2021,** 88, No. 106260.

(18) Choi, J.; Jung, Y.; Yang, S. J.; Oh, J. Y.; Oh, J.; Jo, K.; Son, J. G.; Moon, S. E.; Park, C. R.; Kim, H. Flexible and Robust Thermoelectric Generators Based on All-Carbon Nanotube Yarn without Metal Electrodes. *ACS Nano* **2017,** 11 (8), 7608–7614.

(19) Park, K. T.; Cho, Y. S.; Jeong, I.; Jang, D.; Cho, H.; Choi, Y.; Lee, T.; Ko, Y.; Choi, J.; Hong, S. Y.; Oh, M. W.; Chung, S.; Park, C. R.; Kim, H. Highly Integrated, Wearable Carbon-Nanotube-Yarn-Based

Thermoelectric Generators Achieved by Selective Inkjet-Printed Chemical Doping. *Adv. Energy Mater.* **2022,** 12 (25), No. 2200256.

(20) Sun, T.; Chen, S.; Sun, H.; Li, J.; Wu, X.; Jin, L.; Wang, L.; Jiang, W. Wavy-Structured Thermoelectric Device Integrated with High-Performance n-Type Carbon Nanotube Fiber Prepared by Multistep Treatment for Energy Harvesting. *Compos. Commun.* **2021,** 27, No. 100871.

(21) Abol-Fotouh, D.; Dörling, B.; Zapata-Arteaga, O.; Rodríguez-Martínez, X.; Gómez, A.; Reparaz, J. S.; Laromaine, A.; Roig, A.; Campoy-Quiles, M. Farming Thermoelectric Paper. *Energy Environ. Sci. 2019,* 12 (2), 716–726.

(22) Huo, W.; Xia, Z.; Gao, Y.; Guo, R.; Huang, X. Flexible Thermoelectric Devices with Flexible Heatsinks of Phase-Change Materials and Stretchable Interconnectors of Semi-Liquid Metals. *ACS Appl. Mater. Interfaces* **2023,** 15(24), No. 29330.

(23) Chen, R.; Lee, J.; Lee, W.; Li, D. Thermoelectrics of Nanowires. *Chem. Rev.* **2019,** 119 (15), 9260–9302.

(24) Qiu, L.; Zou, H.; Wang, X.; Feng, Y.; Zhang, X.; Zhao, J.; Zhang, X.; Li, Q. Enhancing the Interfacial Interaction of Carbon Nanotubes Fibers by Au Nanoparticles with Improved Performance of the Electrical and Thermal Conductivity. *Carbon* **2019,** 141, 497–505.

(25) Kim, Y. J.; Park, J.; Jeong, H. S.; Park, M.; Baik, S.; Lee, D. S.; Rho, H.; Kim, H.; Lee, J. H.; Kim, S. M.; Kim, Y. K. A Seed-Mediated Growth of Gold Nanoparticles inside Carbon Nanotube Fibers for Fabrication of Multifunctional Nanohybrid Fibers with Enhanced Mechanical and Electrical Properties. *Nanoscale* **2019,** 11 (12), 5295–5303.

(26) Zhao, K.; Wang, J.; Xie, H.; Guo, Z. Microencapsulated Phase Change N-Octadecane with High Heat Storage for Application in Building Energy Conservation. *Appl. Energy* **2023,** 329, No. 120284.

(27) Niu, S.; Kang, M.; Liu, Y.; Lin, W.; Liang, C.; Zhao, Y.; Cheng, J. The Preparation and Characterization of Phase Change Material Microcapsules with Multifunctional Carbon Nanotubes for Controlling Temperature. *Energy* **2023,** 268, No. 126652.

(28) Yun, J. S.; Choi, S.; Im, S. H. Advances in Carbon-Based Thermoelectric Materials for High-Performance, Flexible Thermoelectric Devices. *Carbon Energy* **2021,** 3 (5), 667–708.

(29) Lan, X.; Wang, T.; Liu, C.; Liu, P.; Xu, J.; Liu, X.; Du, Y.; Jiang, F. A High Performance All-Organic Thermoelectric Fiber Generator towards Promising Wearable Electron. Compos. *Sci. Technol.* **2019,** 182, No. 107767.

(30) Kwon, C.; Lee, S.; Won, C.; Lee, K. H.; Kim, M.; Lee, J.; Yang, S. J.; Lee, M.; Lee, S.; Yoon, K.; Cho, S.; Lee, T. Multi-Functional and Stretchable Thermoelectric Bi2Te3 Fabric for Strain, Pressure, and Temperature-Sensing. *Adv. Funct. Mater.* **2023,** 33, No. 2300092.

(31) An, C. J.; Kang, Y. H.; Song, H.; Jeong, Y.; Cho, S. Y. High-Performance Flexible Thermoelectric Generator by Control of Electronic Structure of Directly Spun Carbon Nanotube Webs with Various

Molecular Dopants. *J. Mater. Chem. A* **2017,** 5 (30), 15631–15639.

(32) Yang, X.; Zhang, K. Direct Wet-Spun Single-Walled Carbon Nanotubes-Based p-n Segmented Filaments toward Wearable Thermoelectric Textiles. *ACS Appl. Mater. Interfaces* **2022,** 14 (39), 44704–44712.

(33) Jang, E.; Banerjee, P.; Huang, J.; Madan, D. High Performance Scalable and Cost-Effective Thermoelectric Devices Fabricated Using Energy Efficient Methods and Naturally Occuring Materials. *Appl. Energy* **2021,** 294, 117006.

(34) Hwang, S.; Jang, D.; Lee, B.; Ryu, Y. S.; Kwak, J.; Kim, H.; Chung, S. All Direct Ink Writing of 3D Compliant Carbon Thermoelectric Generators for High-Energy Conversion Efficiency. *Adv. Energy Mater.* **2023,** No. 2204171.

(35) Lu, Z.; Zhang, H.; Mao, C.; Li, C. M. Silk Fabric-Based Wearable Thermoelectric Generator for Energy Harvesting from the Human Body. *Appl. Energy* **2016,** 164, 57–63.

(36) Li, H.; Zong, Y.; Ding, Q.; Han, W.; Li, X. Paper-Based Thermoelectric Generator Based on Multi-Walled Carbon Nanotube / Carboxylated Nanocellulose. *J. Power Sources* **2021,** 500, No. 229992.

(37) Cao, Z.; Koukharenko, E.; Tudor, M. J.; Torah, R. N.; Beeby, S. P. Flexible Screen Printed Thermoelectric Generator with Enhanced Processes and Materials. *Sensors Actuators, A Phys.* **2016,** 238, 196–206.

(38)Kim, J. Y.; Mo, J. H.; Kang, Y. H.; Cho, S. Y.; Jang, K. S. Thermoelectric Fibers from Well-Dispersed Carbon Nanotube/Poly(Vinyliedene Fluoride) Pastes for Fiber-Based Thermoelectric Generators. *Nanoscale* **2018,** 10 (42), 19766–19773.

(39) Kim, J. Y.; Lee, W.; Kang, Y. H.; Cho, S. Y.; Jang, K. S. Wet-Spinning and Post-Treatment of CNT/PEDOT:PSS Composites for Use in Organic Fiber-Based Thermoelectric Generators. *Carbon* **2018,** 133, 293–299.

(40) Hwang, S.; Jeong, I.; Jeong, I.; Park, J.; Kim, J. K.; Kim, H.; Lee, T.; Kwak, J.; Chung, S. Enhanced Output Performance of All-Solution-Processed Organic Thermoelectrics: Spray Printing and Interface Engineering. *ACS Appl. Mater. Interfaces* **2020,** 12 (23), 26250–26257.